Global atmospheric composition effects from marine isoprene emissions

Article

Accepted Version

Global atmospheric composition effects from marine isoprene emissions

Wentai Zhang,[*,†,‡] James Weber,[¶,§] Alex T. Archibald,[*,‡,‖] Nathan Luke Abraham,[‡,‖] Dennis Booge,[⊥] Mingxi Yang,[#] and Dasa Gu[*,†,@]

†*Division of Environment and Sustainability, Hong Kong University of Science and Technology, Hong Kong, China*

‡*Centre for Atmospheric Science, Yusuf Hamied Department of Chemistry, University of Cambridge, Cambridge, UK*

¶*School of Biosciences, University of Sheffield, Sheffield, UK*

§*Department of Meteorology, University of Reading, Reading, UK*

‖*National Centre for Atmospheric Science, Yusuf Hamied Department of Chemistry, University of Cambridge, Cambridge, UK*

⊥*Marine Biogeochemistry, GEOMAR Helmholtz Centre for Ocean Research Kiel, Kiel, Germany*

#*Plymouth Marine Laboratory, Plymouth, UK*

@*Guangdong-Hongkong-Macau Joint Laboratory of Collaborative Innovation for Environmental Quality, Hong Kong University of Science and Technology, Hong Kong, China*

E-mail: wzhangcn@connect.ust.hk; ata27@cam.ac.uk; dasagu@ust.hk

Abstract

Isoprene emissions, primarily of biogenic origin, play an important role in atmospheric chemistry and climate. However, the atmospheric implications of marine iso-

prene emissions remain underexplored due to sparse in-situ measurements and the intricate mechanisms governing isoprene in the upper ocean. This study uses 20 years of MODIS satellite observations to upscale isoprene production and loss rates derived from laboratory experiments, enabling global modeling of aqueous isoprene concentrations and emissions. Earth system model simulations with integrated marine isoprene emissions demonstrate substantial alterations in atmospheric composition over global oceanic regions. Our investigation uncovers diurnal variation in the vertical profiles of atmospheric isoprene, indicating that surface isoprene can ascend to the mid-to-upper troposphere, where nitrogen monoxide (NO) influences isoprene epoxydiol (IEPOX) production differently over selected oceanic and terrestrial regions. These findings pave the way for future studies on the role of marine isoprene in climate models and advance our understanding of its broader implications for atmospheric chemistry under a changing climate.

Keywords: Isoprene, Earth System Model, Atmospheric Chemistry, Ocean, Satellite Remote Sensing

Synopsis

This study presents global marine isoprene emissions and evaluates their atmospheric chemistry effects using Earth system modeling. The findings reveal that marine isoprene significantly influences atmospheric composition and associated chemical processes.

1. Introduction

Biogenic volatile organic compounds (BVOCs) are important components in atmospheric chemistry, influencing air quality, the greenhouse gases ozone (O_3) and methane, secondary organic aerosols (SOAs), and climate (e.g.,[1]). Among BVOCs, isoprene (C_5H_8) is a major contributor, accounting for approximately half of the global BVOC emissions.[2] Upon reacting

with the hydroxyl radical (OH), O_3, and the nitrate radical (NO_3), isoprene forms species that can contribute to SOA production via reactive uptake[3,4] or volatility driven condensation.[5–8] Recent research has highlighted the significant role of cloud aqueous-phase reactions in SOA production (accounts for about 20% of the total biogenic SOA burden), particularly in the free troposphere.[9] Due to its substantial production and reactivity, isoprene has been identified as a key contributor to global SOA generation.[10–13]

Marine isoprene emissions have been identified for several decades.[14,15] Despite terrestrial vegetation contributing over 90% of global isoprene emissions,[16] emissions directly from the ocean surface dominate isoprene concentrations in the remote marine atmosphere due to isoprene's short atmospheric lifetime (∼hours).[17] Marine isoprene emissions have the potential to be important for SOA formation, especially in eutrophic regions[18,19] and for the organic aerosol marine background.

Phytoplankton is the primary source of isoprene in the upper ocean, and aqueous isoprene shows strong spatial correlations with chlorophyll-a (Chl-a) concentrations and sea surface temperature (SST).[20,21] Isoprene production rates vary with phytoplankton functional types (PFTs),[22,23] and environmental parameters including incident solar radiation and water temperature.[23–26] Isoprene loss processes in seawater include chemical oxidation, microbial consumption, sea-to-air ventilation, and vertical diffusion to the deep ocean.[27] Additionally, photochemical reactions occurring in the sea surface microlayer (SML) represent a significant abiotic isoprene emission source.[28] Current global chemistry-climate models reviewed in IPCC sixth assessment report do not account for marine isoprene emissions, including both biotic (i.e., air-sea exchange driven by isoprene concentration in bulk seawater) and abiotic (e.g., photochemical reactions at the ocean-atmosphere interface) sources.[28] The relative significance of abiotic versus biotic sources remains a topic of ongoing investigation, and a comprehensive understanding of marine isoprene emissions is still a matter of scientific exploration.

The quantification of global marine isoprene emissions faces challenges due to incomplete

knowledge of marine isoprene production mechanisms, uncertainties in laboratory-based production rates, and limited direct flux measurements. Current estimation methods involve bottom-up and top-down approaches. While the bottom-up method focuses on modelling the upper ocean's underlying mechanisms controlling isoprene emissions, the top-down method constrains the model-derived emissions to match atmospheric observations. The two methods yield notably different results, with top-down[29,30] estimates ($1.5 - 11.6\,\mathrm{Tg\,C\,yr^{-1}}$) being remarkably higher than bottom-up[29–33] estimates ($0.1 - 1.2\,\mathrm{Tg\,C\,yr^{-1}}$). The discovery of photochemical production[34] at the ocean surface may partially explain these discrepancies.[35]

Previous model simulations (e.g., CMAQ and GEOS-Chem) have demonstrated the impact of marine isoprene emissions on air quality in coastal and inland regions.[29,30,36,37] However, they have not considered abiotic emissions (e.g., SML emissions) or constrained isoprene concentrations in the bulk seawater, leading to uncertainties in assessing marine isoprene impacts.

This study offers a comprehensive investigation of global marine isoprene emissions and their implications for atmospheric chemistry. We first calculate aqueous isoprene concentrations by employing a recently developed emission scheme[38] with satellite-based data from the Moderate Resolution Imaging Spectroradiometer (MODIS). Our approach incorporates a PFT-specific isoprene production module that accounts for both light and temperature dependency in the vertical aqueous profile. Monthly aqueous isoprene concentrations are derived by balancing phytoplankton production with losses in the water column, assuming a steady-state condition. From these aqueous concentrations, we then calculate marine isoprene emissions and apply these into the United Kingdom Earth System Model (UKESM1) to examine their impact on simulated atmospheric composition.

We validate MODIS-derived seawater isoprene concentrations and UKESM1-simulated atmospheric isoprene mixing ratios by comparison with observations collected during 18 cruise campaigns. Our research explores the ramifications of incorporating these marine isoprene emission schemes on atmospheric chemistry, shedding new light on the important

role of marine isoprene in affecting the Earth's atmosphere.

2. Materials and Methods

2.1 MODIS and satellite products

The MODIS instrument, launched aboard NASA's Earth Observing Satellites (EOS), offers extensive global coverage with a broad swath width of 2330 km in a single day. It operates in 36 high spectral resolution channels spanning wavelengths from 0.415 to 14.235 μm, providing spatial resolutions of 250 m (2 channels), 500 m (5 channels), and 1000 m (29 channels). MODIS radiance measurements at high spatial resolution provide valuable information about the Earth's atmosphere and surface structure.[39] This study utilized monthly MODIS products, including Chl-a, SST, and Photosynthetically Active Radiation (PAR), as well as near-real-time Mixed Layer Depth (MLD) products[40,41] and wind speed from the European Center for Medium-Range Weather Forecasts (ECMWF) ERA5 reanalysis,[42] spanning from July 2002 to December 2021. Global PFT distributions during the same period were retrieved using the PHYSTWO method, derived from MODIS products: the Chl-a concentration, the aerosol optical thickness (AOT) at 865nm, and remote sensing reflectances at 412 nm, 443 nm, 469 nm, 490 nm, 531 nm, 547 nm, 555 nm.[43] Monthly global seawater isoprene concentrations and emission fluxes from July 2002 to December 2021 were calculated using the emission scheme based on MODIS data. These results were then used to establish climatologies of aqueous isoprene and emission fluxes.

2.2 Marine isoprene emission scheme

The emission scheme employed here uses a set of parameters, including Chl-a, SST, PAR, MLD, PFT, and wind speed, to derive marine isoprene fluxes.

As the isoprene concentrations in the mixed layer do not change significantly on a weekly basis,[44] the monthly mean isoprene concentration C_w can be estimated by solving the mass

balance in the steady-state water column of the upper ocean:

$$P - (k_{bio} + k_{chem}) \cdot C_w - \frac{F_{ocean}}{D_{ML}} - L_{mix} = 0 \quad (1)$$

where P is the isoprene variation rate induced by the phytoplankton production, k_{bio} and k_{chem} is the biological loss rate (day^{-1}) and chemical rate constant (day^{-1}) for all possible loss pathways. D_{ML} is the surface mixed layer depth (m), and L_{mix} is the loss due to the diffusion downward to the deep ocean ($\mathrm{pmol\,L^{-1}\,day^{-1}}$). P can be derived by integrating the isoprene production rate within the depth H:

$$P = \frac{\beta}{D_{ML}} \cdot \overline{[Chla]} \cdot \int_0^H p\, dh \quad (2)$$

where β is the acclimation prefactor, $\overline{[Chla]}$ is the mean Chl-a concentration ($\mathrm{mg\,m^{-3}}$) within the euphotic layer (depth H_{max}), H is the minimum of H_{max} and D_{ML} both in meters, and p is the isoprene production rate ($\mu\mathrm{mol\,gChla^{-1}\,h^{-1}}$). This production rate incorporates the PFT-specific emission factor, water temperature, and ambient solar radiation.[38] The emission factor for each PFT is derived using a log-squared fit to relate the [Chl-a]-normalized isoprene production rates measured during the incubation experiments to incident radiation levels.[21,45] Light dependence follows the log-squared relationship proposed by Gantt et al.[45], with radiation at various seawater depths estimated using the Beer-Lambert's Law applied to solar radiation at the sea surface. The temperature-dependence factor is derived empirically from temperature-dependent experiments and is adjusted according to the optimum temperature, which is a function of latitude. To enhance the practical applicability of our scheme in oceanic environments, β was calibrated by aligning the mean value of estimated C_w with that of measurements obtained during the AMT22 campaign (see Figure 1 and Table S1). For validation purposes, our analysis exclusively considered atmospheric isoprene collected in open ocean regions (defined in Figure S1), as coastal zones may be subject to influence from terrestrial sources.[29]

The marine isoprene emission flux, F (in $\mathrm{nmol\,m^{-2}\,hour^{-1}}$), is described as the sum of ocean-atmosphere exchange flux F_{ocean} and SML flux F_{SML}:

$$F = F_{ocean} + F_{SML} \tag{3}$$

F_{ocean} (in $\mathrm{nmol\,m^{-2}\,hour^{-1}}$) can be estimated from the isoprene concentration (in $\mathrm{pmol\,L^{-1}}$) in the bulk seawater:[31]

$$F_{ocean} = k_{AS} \cdot (C_w - C_a \cdot H^{-1}) \tag{4}$$

where k_{AS} is the air-sea gas transfer coefficient (in $\mathrm{m \cdot s^{-1}}$) which considers the loss processes due to air-sea gas exchange, C_a is the atmospheric isoprene concentration, and H is the dimensionless Henry's law constant for isoprene (i.e., the ratio of C_a to C_w at equilibrium). The parameterization reported by Wanninkhof[46] is used to compute k_{AS} (in $\mathrm{cm \cdot h^{-1}}$):

$$k_{AS} = 0.251 \cdot \overline{U_{10}^2} \cdot (\frac{660}{S_C})^{0.5} \tag{5}$$

where U_{10} (in $\mathrm{m \cdot s^{-1}}$) represents the wind speed at 10 meters above the surface, and $\overline{U_{10}^2}$ is the average of the squared U_{10}. Following Rodríguez-Ros et al.[47], this study uses the square of the monthly mean wind speed due to the lack of hourly wind speed data in the UKESM1 CMIP6 archive and for faster computation. The average difference between $\overline{U_{10}^2}$ and $\overline{U_{10}}^2$ in our analysis is 10.85% (see Section S3). The Schmidt number (Sc, dimensionless) is calculated using the relationship given by Palmer and Shaw[31]:

$$S_c = 3913.15 - 162.13 \cdot T + 2.67 \cdot T^2 - 0.012 \cdot T^3 \tag{6}$$

where T is the SST in degree Celsius (°C).

Photochemical experiments have been conducted in the laboratory on both synthetic and authentic SML samples.[34] The SML isoprene flux, F_{SML} (in $\mathrm{nmol\,m^{-2}\,hour^{-1}}$), can be

estimated by scaling up the net photochemical emission rate of isoprene per unit power measured in the laboratory, F_{lab} (in molecules of isoprene $\mathrm{mW}^{-1} \cdot \mathrm{s}^{-1}$), using a scaling factor μ_{photo}:

$$F_{SML} = \mu_{photo} \cdot F_{lab} \tag{7}$$

Here, μ_{photo} (in $\mathrm{mW} \cdot \mathrm{m}^{-2}$) is the photochemical emission potential.[35] For this study, F_{lab} is set to 4.95×10^7 molecules $\mathrm{mW}^{-1} \cdot \mathrm{s}^{-1}$, which is the mean value of the reported range $3.71 - 6.19 \times 10^7$ molecules $\mathrm{mW}^{-1}\mathrm{s}^{-1}$.[33]

The photochemical emission potential is used to calibrate the oceanic conditions to the standard laboratory environment by incorporating three key parameters: surfactant concentration in the SML, wind speed, and ultraviolet (UV) solar radiation (280–400 nm). Other potential factors, such as the specific identity of surfactant and the thickness of the SML, are not included in this study due to the absence of established parameterizations. The net photochemical isoprene flux is assumed to have a linear relationship with solar radiation.[48] Laboratory studies typically use the 280–400 nm wavelength range to determine the net photochemical emission rate per unit power.[48] This wavelength range is chosen because shorter wavelengths may induce photolysis, while longer wavelengths lack sufficient energy to drive photochemical reactions. The photochemical emission potential, μ_{photo}, is expressed as the product of these three parameters, as shown in the following equation:

$$\mu_{photo} = F_{surf} \cdot k_{SML} \cdot E_{280-400} \tag{8}$$

where $E_{280-400}$ represents the ultraviolet solar radiation (280-400 nm) reaching the sea surface. In this study, $E_{280-400}$ is set to a constant proportion (4.3%) of the surface downwelling solar radiation due to the lack of diagnostic variable for UV radiation from UKESM1 CMIP6 archive.[49] F_{surf} is a correction factor accounting for spatial variations in surfactant concentrations within the SML. It is based on the logarithmic relationship between the isoprene

yield and surfactant concentrations found in laboratory experiments:[34,35,50]

$$F_{surf} = \frac{\ln\left(c_{surf}\right)}{\ln\left(c_{max,surf}\right)} \tag{9}$$

Here, c_{surf} denotes the surfactant concentration in the SML, assigned to the mean values observed in three trophic states of the sampling areas, as reported by Wurl et al.[51]. For oligotrophic waters, $c_{surf} = 320\,\mu\mathrm{g\,Teq\cdot L^{-1}}$; for mesotrophic waters, $c_{surf} = 502\,\mu\mathrm{g\,Teq\cdot L^{-1}}$; and for eutrophic waters, $c_{surf} = 663\,\mu\mathrm{g\,Teq\cdot L^{-1}}$. Trophic states are classified based on net primary production (NPP): oligotrophic waters have NPP $< 0.4\,\mathrm{g\,C\,m^{-2}\cdot day^{-1}}$; mesotrophic waters have NPP between 0.4 and 1.2 $\mathrm{g\,C\,m^{-2}\cdot day^{-1}}$; and eutrophic waters have NPP $> 1.2\,\mathrm{g\,C\,m^{-2}\cdot day^{-1}}$. The maximum surfactant concentration, $c_{max,surf}$, is set at 663 $\mu\mathrm{g\,Teq\cdot L^{-1}}$. NPP values were calculated following the method described in Wurl et al.[51].

The gas transfer coefficient, k_{SML}, varies with wind speed and is normalized to laboratory conditions by using the parameterization of McGillis et al.[52] as follows[35]:

$$k_{SML} = \frac{8.2 + 0.014 \cdot U_{10}^3}{8.2 + 0.014 \cdot U_{lab}^3} \cdot H(U_{10}) \tag{10}$$

where U_{10} is the wind speed at 10 meters above the sea surface, and U_{lab} is the sample flow speed under laboratory conditions, set at $U_{lab} = 5.31 \times 10^{-2}\,\mathrm{m\cdot s^{-1}}$. It should be noted that the surfactant in the SML is photochemically active at moderate wind speeds below $13\,\mathrm{m\cdot s^{-1}}$[53]. Above this threshold, the SML disperses, rendering the SML emissions negligible. To account for the presence or absence of the SML at a given U_{10}, we define the step function $H(U_{10})$ as follows:

$$H(U_{10}) = \begin{cases} 1, & \text{if } U_{10} \leq 13\,\mathrm{m\cdot s^{-1}} \\ 0, & \text{if } U_{10} > 13\,\mathrm{m\cdot s^{-1}} \end{cases} \tag{11}$$

This parameterization ensures that the isoprene photochemical emissions is restricted to conditions where SML is physically present.

2.3 UKESM1 model description and setup

All simulations in this study utilized UKESM1 and were conducted using the atmospheric component of the model within the Atmospheric Model Intercomparison Project (AMIP) configuration. The model was configured at a horizontal resolution $1.25^\circ \times 1.875^\circ$ with 85 vertical levels extending up to 85 km. These simulations incorporated fully interactive stratospheric and tropospheric chemistry, including interactive oxidants, using the CRI-Strat 2 (CS2) mechanism,[54] which implements updated isoprene chemistry.[55] The GLOMAP-mode aerosol scheme was employed to represent various aerosol types, including sulfate (SO_4^{2-}), sea-salt, black carbon, primary organic aerosol (POA), SOA and dust. The yield of SOA from monoterpene was enhanced from 13% in Mann et al.[56] to 26% to account for the lack of SOA, as was done in UKESM1 simulations conducted for CMIP6.[57] It is important to note that nitrate aerosol was not included in these simulations.[58] To prevent diverging meteorology from adding to the differences resulting from the chemical mechanisms and to replicate the atmospheric conditions experienced when the observations were recorded as closely as possible, temperature and horizontal wind fields were nudged in all model runs.[59] Nudging was implemented using atmospheric reanalysis data from ECMWF[60] and was confined to altitudes above approximately 1200 meters. A more comprehensive description of the model's mechanisms and configurations are provided by Mulcahy et al.[61]. The details on the UKESM1 simulations are available in Section S1.

3. Results and discussion

3.1 Isoprene pool in the upper ocean

Estimated isoprene concentrations within the upper ocean display pronounced seasonality and latitudinal gradients (Figure S2). Notably, the tropical ocean consistently maintains higher aqueous isoprene levels throughout the year. In particular, the eastern equatorial Pacific Ocean experiences the highest isoprene levels between February and April. Similarly, the Arabian Sea near Oman has elevated concentrations in March. During the northern hemisphere (NH) summer, isoprene concentrations reach their peak in the Arctic and along the middle-to-high northern latitude coastal areas. Conversely, the Southern Ocean has the lowest isoprene concentrations during this season and much higher concentrations in the austral summer. Detailed methodologies for deriving isoprene concentrations in bulk seawater can be found in the Methods section.

3.2 Evaluation of aqueous isoprene

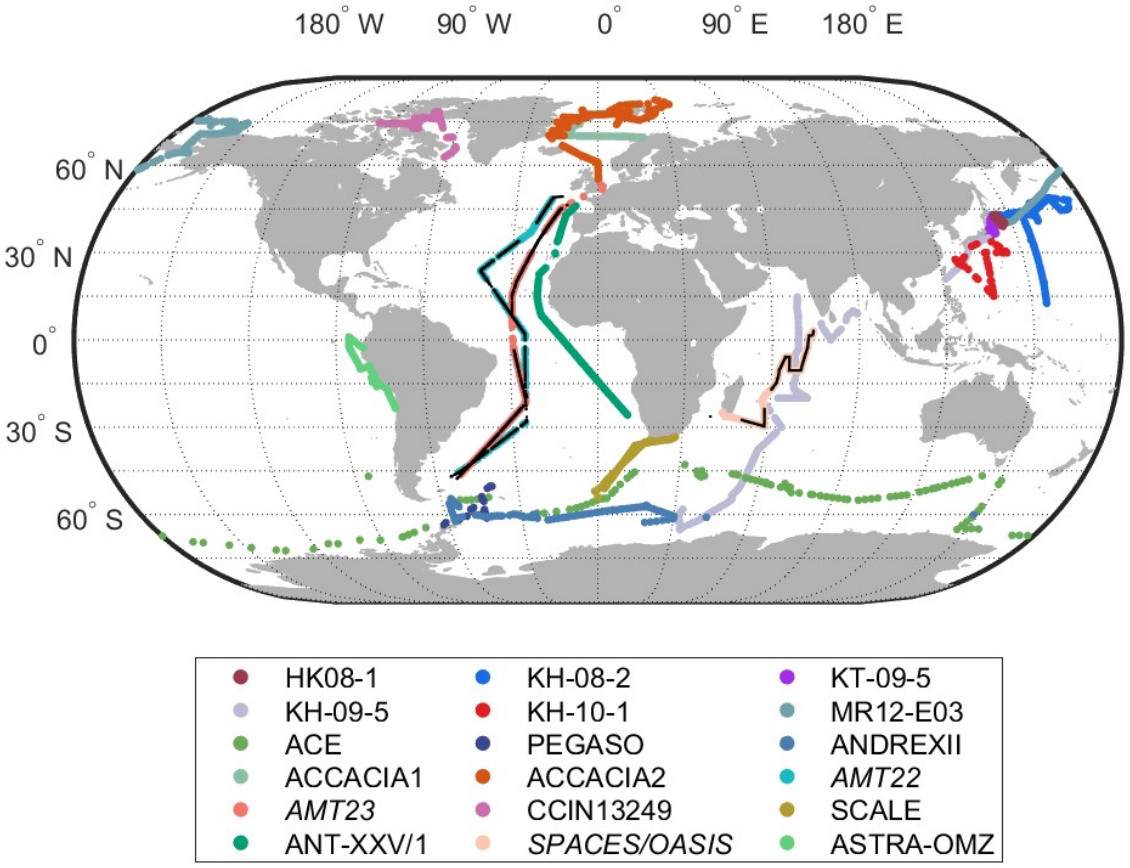

Figure 1: Sampling sites of seawater (dots in color) and marine air (dots in black) during the cruise campaigns used in this study. The cruise IDs in italics denote the availability of atmospheric measurements. The black dots over colored dots represent the air sampling sites of the cruise in the open ocean, as defined in Figure S1. Further information about the cruises is provided in Table S1.

Our marine isoprene emission scheme underwent a rigorous validation process using cruise measurements from various oceanic regions. Figure S3 presents a density scatter plot illustrating the scheme's performance in estimating isoprene concentrations in the upper ocean. Our scheme achieved a significant correlation, with an R-squared value of 0.47 and a slope of 0.92 (p-value: 0). This analysis was based on a dataset of 6839 valid seawater measurements collected during 18 cruise campaigns (Figure 1). The measurements were taken at depths of 2-7 meters across a diverse range of oceanic environments and analyzed using various instruments, forming the foundation of our evaluation. This emission scheme was then used

to generate marine isoprene emissions which were included in UKESM1 simulations. For a more in-depth examination of the scheme's performance during each individual cruise campaign, we invite readers to refer to the detailed comparisons presented in Figure S4, S5, and S6.

3.3 Marine isoprene emission fluxes

The average annual marine isoprene emission from 2003 to 2021 is $0.8943 \pm 0.0114\,\mathrm{Tg\,C\,yr^{-1}}$, with ocean-atmosphere exchange flux at $0.2681 \pm 0.0052\,\mathrm{Tg\,C\,yr^{-1}}$ and SML emission flux at $0.6340 \pm 0.0067\,\mathrm{Tg\,C\,yr^{-1}}$. Seawater isoprene fluxes and SML fluxes from the global ocean exhibit distinct seasonal patterns (Figure 2A-H). Emissions are lowest in June and peak in January (Figure 2I), highlighting the Southern Hemisphere's crucial contribution to annual global emissions (Figure S7). The highest flux occurs between 45°S to 65°S during December to January (austral summer). Several other high-emission areas are notable during this period: the near-shore region of Western Australia, the eastern equatorial Pacific Ocean, the Southern Atlantic Ocean near southern Africa, and waters off Somalia. The Norwegian Sea shows elevated emissions from May to August, which aligns with the broader seasonal patterns observed.[15] Detailed methodologies for calculating emission fluxes can be found in the Methods section.

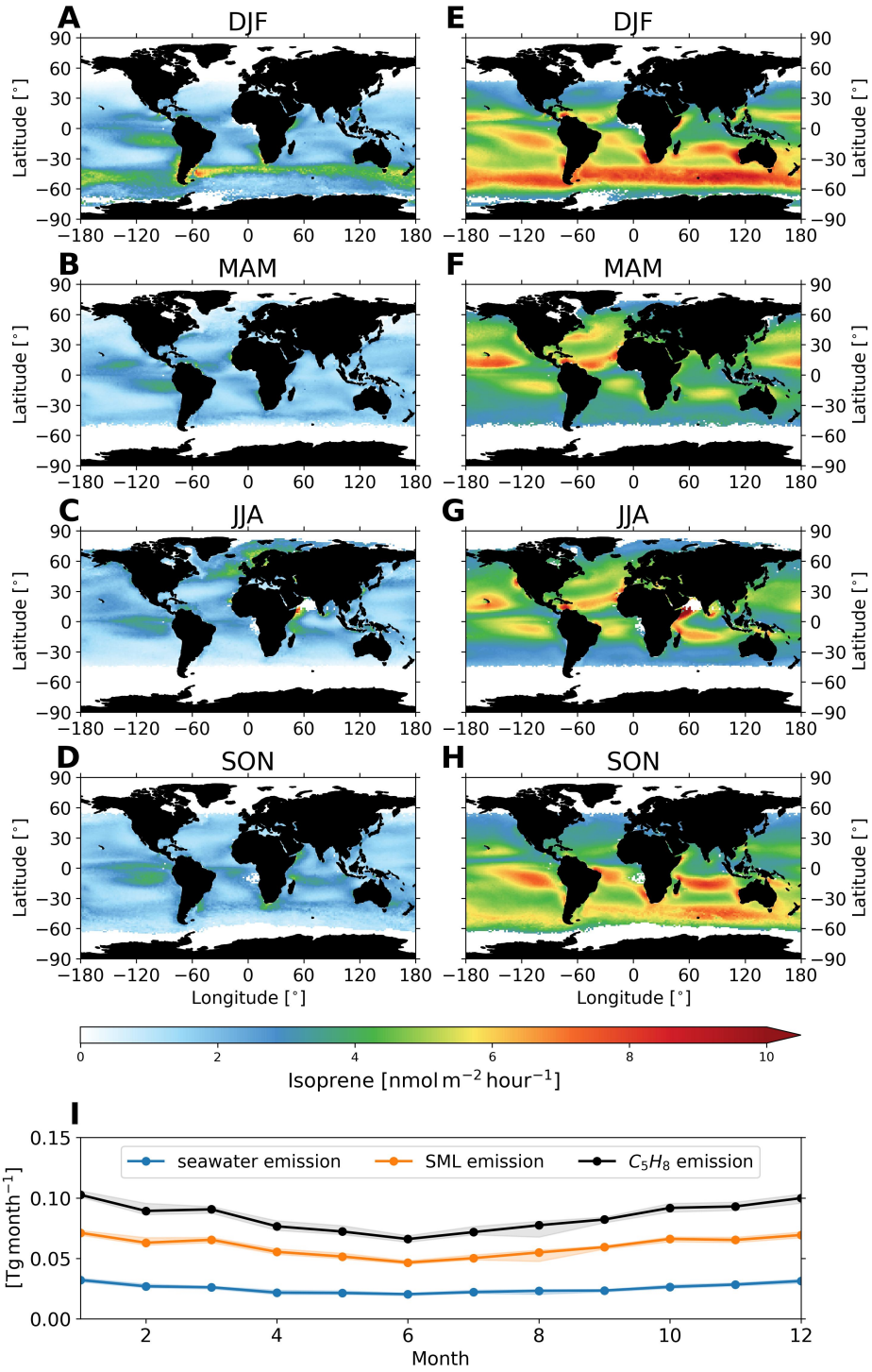

Figure 2: Marine isoprene emission fluxes by season, calculated from MODIS data (July 2002 - December 2021). Seawater fluxes: (A) Dec-Feb, (B) Mar-May, (C) Jun-Aug, (D) Sep-Nov. SML fluxes: (E) Dec-Feb, (F) Mar-May, (G) Jun-Aug, (H) Sep-Nov. (I) climatological global emissions, with shaded areas showing monthly flux maxima and minima.

3.4 Evaluation of atmospheric isoprene

To evaluate the simulated atmospheric isoprene, we conducted two UKESM1 simulations, named "cruise_comparison" and "cruise_10×comparison". These simulations included "bottom-up" and "10-scaled" marine isoprene emissions, respectively (Table S2). The sole difference between the two simulations is that "cruise_10×comparison" used marine isoprene emissions scaled to ten times those in the "cruise_comparison" simulation. We extracted the hourly atmospheric isoprene mixing ratios at the grid points closest to the atmospheric sampling sites of the three cruise campaigns (AMT22, AMT23, SPACES/OASIS) (see Figure 1) at corresponding times for our evaluation.

We performed a linear regression analysis of the surface atmospheric isoprene mixing ratios from the "cruise_comparison" and "cruise_10×comparison" simulations against measurements from the three cruises, incorporating 742 valid atmospheric measurements. To ensure the reliability of our comparison, we restricted the analysis to measurements taken in the open ocean (as defined in Figure S1), thereby mitigating the influence of terrestrial isoprene. The analysis for the "cruise_comparison" simulation revealed a strong correlation, with an R-squared value of 0.58 and a slope of 0.104 (p-value: 6.95e-137). This indicates a consistent underestimation of isoprene mixing ratios by the simulation, approximately by a factor of 10, when compared to atmospheric measurements (Figure S8). The "cruise_10×comparison" simulation also showed a strong correlation, with an R-squared value of 0.51 and a slope of 1.083 (p-value: 8.09e-160). This demonstrated that the tenfold scaling in the "cruise_10×comparison" simulation effectively addressed the low bias of atmospheric isoprene found in the "cruise_comparison" simulation.

It is crucial to note that Figure S3 addresses the parameterization of isoprene concentration in bulk seawater, driven by biotic sources and is unaffected by the SML source. Conversely, Figure S8 reflects the combined influence of both biotic and SML emissions from the surface ocean.

3.5 Atmospheric implications

To assess the impact of including marine isoprene emissions on atmospheric chemical composition, simulations were performed with the UKESM1 (Table S2). Specifically, a simulation with isoprene emissions solely from terrestrial sources ("land_only") served as the control and as a point of comparison for multiple simulations with different approaches to model marine isoprene emissions. Simulated surface atmospheric isoprene concentrations in UKESM1 simulations using bottom-up emissions ("land_marine") were low-biased by around a factor of 10 (Figure S8). Multiplying the bottom-up emissions by 10 makes the simulated surface isoprene level ∼10 times higher (Table S3), generating a "top-down" emissions. Therefore, a further run ("land_10×marine") was performed with the "top-down" emissions and this served as the primary point of comparison with the "land_only" control.

Surface atmospheric isoprene increases of up to 40 ppt are simulated during 2006 in the latitude range of $45°S - 65°S$ (Figure 3A), highlighting the large contribution of isoprene emissions in this region to the surface atmospheric burden. Surface levels of OH decrease in oceanic areas (Figure 3B). This decrease signifies a reduction in oxidative capacity in the surface atmosphere, primarily due to the reaction of marine isoprene with OH. In contrast, surface O_3 levels exhibit slight increases across most oceanic regions (Figure 3C and Figure S9A). This is likely due to the reduced reaction of OH with O_3, leading to an increase in O_3 concentrations.[62] Although isoprene can react directly with O_3, reducing its atmospheric levels, the high reaction rate of isoprene with OH and the coincidence of peak in OH and isoprene concentrations during the day suggest that the OH-pathway is the more important isoprene oxidation pathway.[63] Surface formaldehyde (HCHO) and methanol (CH_3OH) levels also increase in most oceanic areas (Figure 3D&E and Figure S9B&C), highlighting their roles as products in the isoprene oxidation pathway. Simulated changes in surface isoprene epoxydiols (IEPOX) mixing ratios exhibit values that are three orders of magnitude lower than those of isoprene (Figure 3, A and F), suggesting that other chemical pathways, such as RO_2 isomerization and $RO_2 + RO_2$ reactions, dominate the fate of isoprene RO_2 radicals

(ISOPO$_2$) under low-NO$_x$ conditions.[64] Furthermore, relative changes in IEPOX mixing ratios indicate that marine IEPOX dominates over the transported IEPOX from terrestrial isoprene sources in the open ocean (Figure S9D).

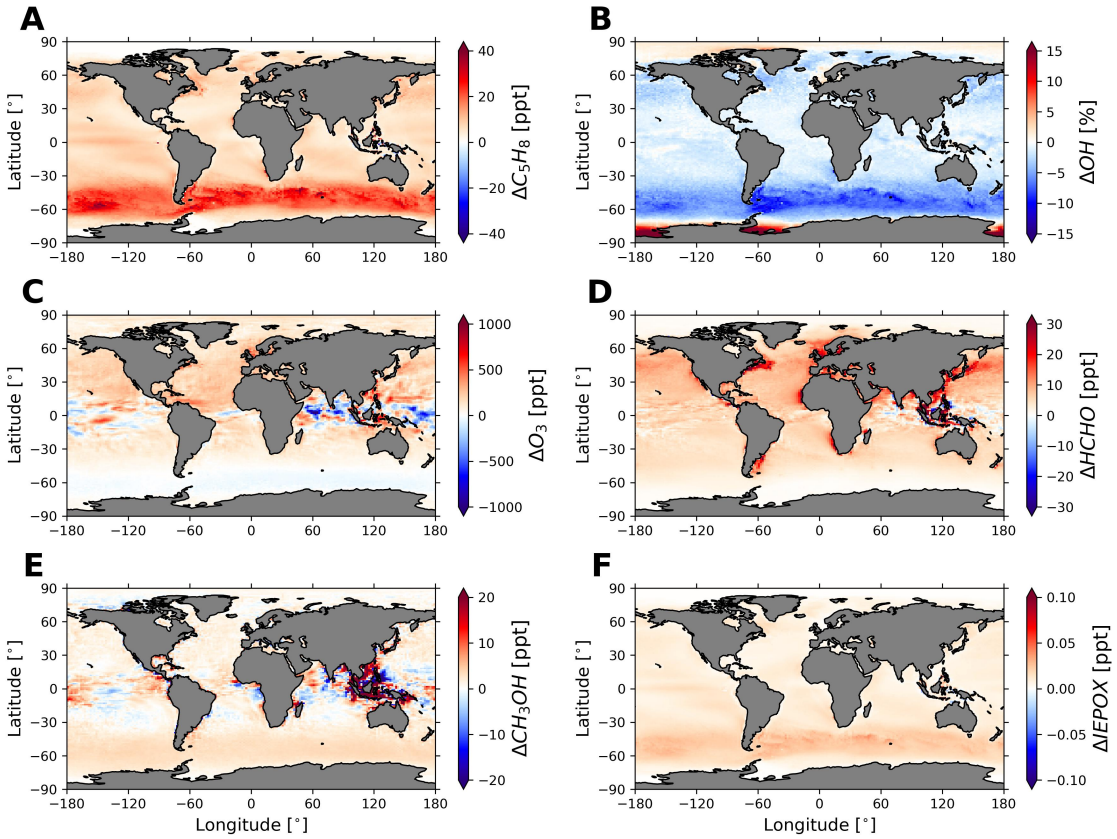

Figure 3: The averaged change in surface atmospheric components in 2006, derived from the simulation "land_10×marine" and "land_only". (A) change in surface C_5H_8 mixing ratio (in pptv), (B) change in surface OH mixing ratio (in percentage), (C) change in surface O_3 mixing ratio (in pptv), (D) change in surface HCHO mixing ratio (in pptv), (E) change in surface CH_3OH mixing ratio (in pptv), (F) change in surface IEPOX mixing ratio (in pptv).

Zonally, isoprene concentrations exhibit increases over the open ocean (defined in Figure S5) within the lowest $\sim$ 1 km (Figure 4A). O_3 changes are more pronounced in tropical regions (Figure 4C), while the changes in HCHO mirror those of OH (Figure 4, B and D). IEPOX increases at the surface and also in the tropical upper troposphere (Figure 4E). Additionally, CH_3OH shows large increases throughout most of the troposphere (Figure 4F). Further discussion on how emission uncertainties affect atmospheric composition is provided

in Section S2 and Figure S10-S15.

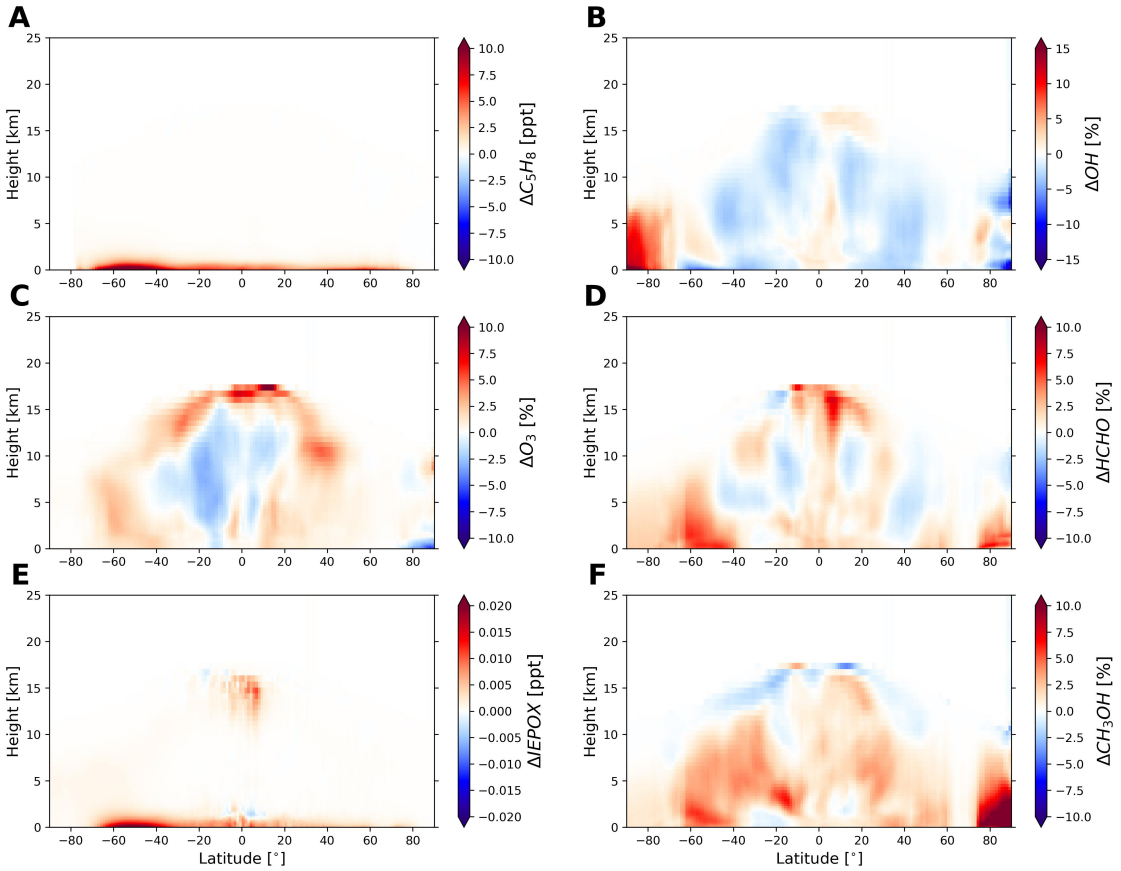

Figure 4: Model-simulated zonal mean change of atmospheric components in the troposphere over the open ocean in 2006, derived from the simulation "land_10×marine" and "land_only". (A) change in C_5H_8 mixing ratio (in pptv), (B) change in OH mixing ratio (in percentage), (C) change in O_3 mixing ratio (in percentage), (D) change in HCHO mixing ratio (in percentage), (E) change in IEPOX mixing ratio (in pptv), (F) change in CH_3OH mixing ratio (in percentage).

To gain insight into the vertical distribution of isoprene and its oxidation products, we examined their mean vertical profiles in a selected oceanic and land region, as defined in Figure S16. Hourly profiles from April 2014 (shown in Figure 5 for the oceanic region and Figure S18 for the land region) were averaged to derive daily diurnal variations (Figure S19 for the oceanic region and Figure S20 for the land region).

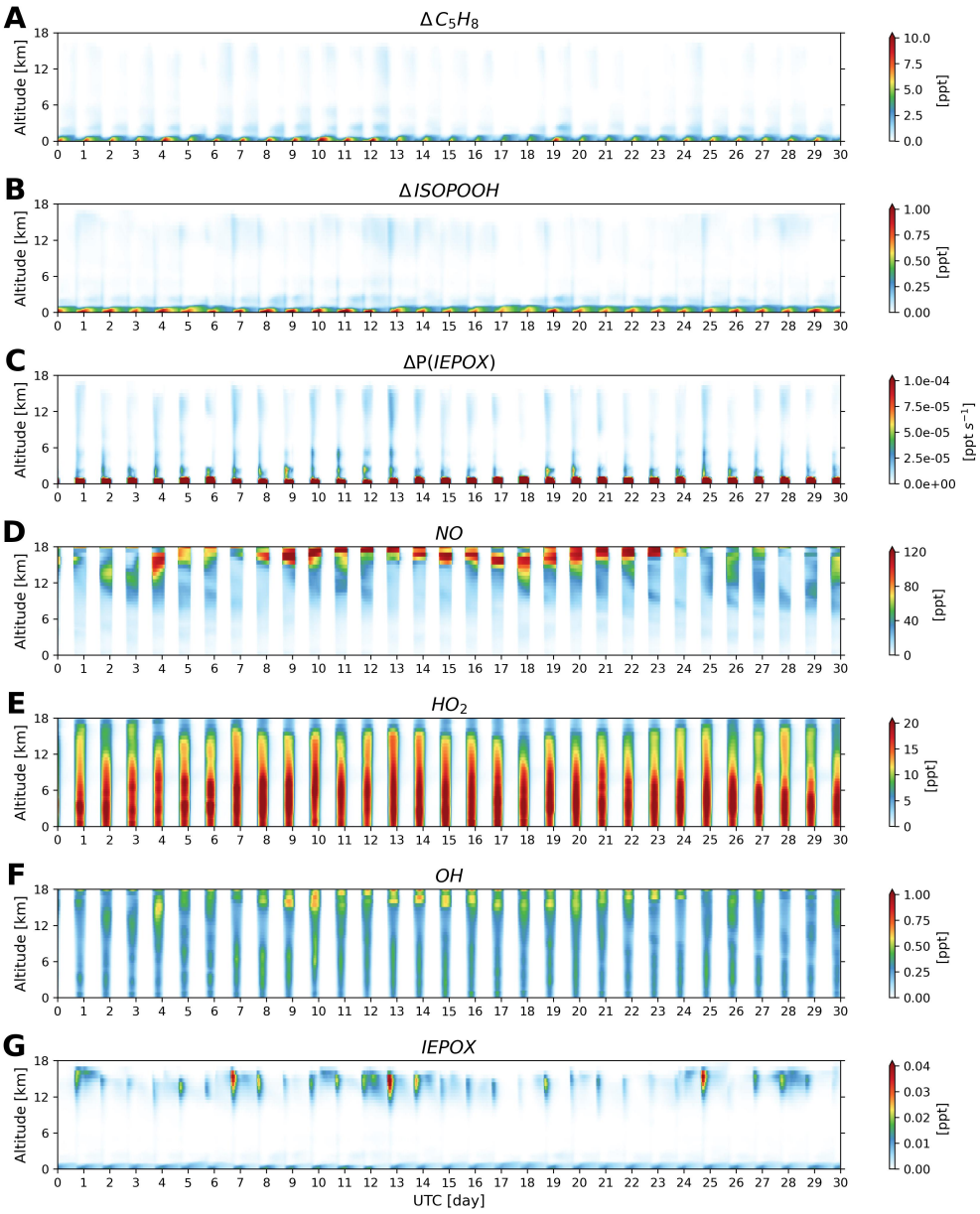

Figure 5: UKESM1 hourly analysis of the profile of marine isoprene, and selected gas-phase oxidation products, NO, HO_2, and OH over the selected ocean region during April 2014. The region is defined as 150°W to 145°W and 12°S to 6°S and is denoted by the rectangle in Figure S10. (A) ΔC_5H_8 (pptv). (B) ΔISOPOOH (pptv). (C) ΔProduction rate of IEPOX ($ppt\,s^{-1}$). (D) NO (pptv). (E) HO_2 (pptv). (F) OH (pptv). (G) IEPOX (pptv). Time is indicated as days of April in Coordinated Universal Time (UTC). Profiles in (A-C) are derived from the difference (Δ) between the simulation "hourly_profile" and "hourly_land_only", while profiles in (D-G) stem solely from the "hourly_profile" simulation. It is noteworthy that the profile changes in (A-C) are positive and IEPOX in "hourly_land_only" is negligible over this region (see Figure S17).

Our results indicate that marine isoprene can accumulate in the planetary boundary layer (PBL) post-sunset, ascending to the free troposphere during the nighttime (Figure 5A and Figure S19A). The nighttime lifetime of isoprene is largely influenced by reactions with O_3 and NO_3, while isoprene in daytime conditions is primarily governed by OH oxidation. The extended lifetime of isoprene during the nighttime leads to elevated isoprene levels in the troposphere. Furthermore, isoprene hydroxyl hydroperoxide (ISOPOOH) levels in the PBL follow a distinct diurnal pattern, increasing at sunrise, peaking at sunset, and subsequently declining, reflecting a close relationship with OH levels (Figure 5B and Figure S19B). At sunrise, the isoprene that survived the night initiates the formation of ISOPOOH and IEPOX, influenced in part by hydroperoxyl radicals (HO_2). Elevated nitrogen oxide (NO) levels correlate with reduced IEPOX production in the upper troposphere (Figure 5, C and D) due to the competition between the reactions of NO and HO_2 with isoprene peroxy radicals ($ISOPO_2$),[65] both of which occur throughout most of the global atmosphere.[64] Only the reaction with HO_2 produces ISOPOOH, leading to IEPOX formation. When NO concentrations are low, HO_2 predominantly reacts with $ISOPO_2$, enhancing ISOPOOH and subsequently IEPOX production (Figure S19). Given that OH concentrations in this region are higher than ISOPOOH (Figure 5, B and F), the OH formed from NO reactions does not significantly affect IEPOX formation. This indicates that NO primarily influences IEPOX formation by reacting with $ISOPO_2$, offering a competitive pathway that can suppress IEPOX formation. The prolonged lifetime of isoprene oxidation products, such as IEPOX(Figure 5G), enable long-range transport, which can lead to wider impacts for atmospheric chemistry and the formation of SOAs in remote regions.

Similarly, terrestrial isoprene in selected land regions (as defined in Figure S16) maintains high levels in the PBL, exceeding 10 ppb, and ascends to the mid-to-upper troposphere during nighttime (Figure S18A and Figure S20A). Enhanced upper tropospheric NO leads to increased IEPOX mixing ratios at corresponding altitudes (Figure S18C-G and Figure S20C-F). In this region, ISOPOOH concentrations are three orders of magnitude higher than

OH concentrations (Figure S18, B and F), allowing OH formed from NO to significantly facilitate the oxidation of ISOPOOH, thereby generating IEPOX.[66] The highest level of upper tropospheric ISOPOOH are observed right before sunrise, likely due to the transport of isoprene from the boundary layer during the nighttime (Figure S20A&B). The distinct relationship between NO and IEPOX abundance in the upper troposphere over the selected ocean and land regions suggests the nonlinear effects of NO_x on the formation of isoprene-derived SOA in the ambient atmosphere.[65]

3.6 Missing isoprene source at the air-sea interface?

The three cruises (AMT22, AMT23, and SPACES/OASIS) have yielded comprehensive data on both seawater and atmospheric concentrations of isoprene. Our estimations of seawater isoprene concentrations demonstrate strong agreement with measurements gathered during these cruises. However, despite incorporating a bottom-up emission—comprising seawater emission flux and SML emission flux—we note a conspicuous disparity between simulated and observed atmospheric isoprene concentrations across each individual cruise campaign.

The distinction between a point location (representing measurement) and a grid cell, potentially rendering cruise air measurements unrepresentative, should be acknowledged as potential contributor to the observed low bias. However, the difference between measurement height and UKESM1 model surface level does not fully explain the observed discrepancies. The sampling elevation during all three cruises (18-20 m above sea level) falls well within the model surface layer (0-36 m over the ocean) and closely aligns with the height of the first model level (20 m over the ocean). Comparisons between simulated outputs and ATOM aircraft campaign measurements at altitudes below 1 km show good agreement in O_3 mixing ratios, but simulated OH levels are approximately twice the observed values. Additionally, the underestimation of isoprene may be related to challenges in accurately simulating marine boundary layer height and mixing processes.

The well-matched aqueous isoprene concentrations suggest that the seawater flux esti-

mates are likely robust. In contrast, the SML flux estimates, upscaled from laboratory measurements of both artificial samples and authentic SML samples,[34] require further constraints through in-situ measurements. Analysis of the ratio between modeled and observed isoprene mixing ratios against seawater and SML fluxes during the three cruise campaigns indicates that the potential missing isoprene source is more influenced by the SML flux. This is evidenced by the larger slope and lower y-intercept of the regression line for SML flux compared to seawater flux (see Figure S21). Notably, improving SML emission estimates may depend critically on accurate measurements of the UV radiation fraction over oceanic regions. Uncertainty analysis shows that the UV fraction is the largest source of uncertainty in marine isoprene emission estimations (see Table S4). The UV fractions used for SML flux calculations (4.3% as stated in the methods section, and 2.9% $\sim$ 7.7% in sensitivity tests) were derived from land-based measurements due to the lack of ocean-specific data. However, it is possible that oceanic UV fractions are higher, as water vapor—abundant in marine environments—absorbs UV radiation less efficiently than aerosols,[49] which are generally more concentrated over terrestrial regions.

Therefore, our UKESM1 simulations reveal that marine isoprene emissions could exceed our bottom-up emission estimates. The atmospheric isoprene levels from the two simulations, "land_marine" and "cruise_comparison", should be considered as minimum mixing ratios, very likely being higher in reality and therefore having more profound implications for atmospheric chemistry.

3.7 Potential climate impacts

While prior GEOS-Chem simulations including 2% SOA gas-phase yield from bottom-up ($0.31\,\mathrm{Tg\,yr^{-1}}$) and top-down ($1.9\,\mathrm{Tg\,yr^{-1}}$) emissions have shown that marine isoprene plays an insignificant role in remote marine aerosol abundances,[29] the higher marine isoprene emissions reported in our study (bottom-up emissions $0.89\,\mathrm{Tg\,C\,yr^{-1}}$, top-down emissions $8.9\,\mathrm{Tg\,C\,yr^{-1}}$) and the larger multiphasic SOA yield values ($\sim$4%) revealed by a recent

chamber experiment and modeling study[9] collectively suggest a larger contribution to marine aerosols. The transport of surface isoprene and its oxidation products to the upper troposphere highlighted in Figure 5 and Figure S18 could lead to interactions with cirrus clouds which play an important role in the Earth's radiation budget.[9,67] Both chamber experiments[68] and aircraft measurements[69] have revealed upper tropospheric new particle formation, which represents a globally important source of atmospheric aerosols. Our sensitivity experiments further reveal that uncertainties in marine isoprene emissions result in variations in the ratio of tropospheric IEPOX burden over open ocean to that over land, ranging from 0.38% to 1.94% (see Table S5). This sensitivity also suggests that marine IEPOX could be at least comparable to terrestrial IEPOX over open ocean, with OH oxidation being the dominant pathway for IEPOX loss in the low-NO_x marine atmosphere. Such uncertainties hinder the use of organic compounds in ice cores as reliable marine biomarkers for reconstructing past environmental conditions.[70] Therefore, more accurate estimates of marine BVOC emissions are crucial for correctly interpreting ice core records. As the isoprene-derived SOAs (e.g., IEPOX SOAs) have been identified to play a role in the nucleation of ice particles,[67] marine isoprene emissions could affect weather and climate by influencing precipitation efficiency and cloud formation. It would be very valuable to perform studies that address the climate feedback parameter of marine isoprene emissions, as it may differ in size and sign from those derived for terrestrial emissions.[1,71]

Author Information

Author Contributions

Conceptualization: W.Z, J.W., A.A., D.G. Methodology: W.Z., J.W., A.A. Software: W.Z., J.W., A.A., N.L.A. Formal Analysis: W.Z., J.W. Data Curation: W.Z., J.W., D.B., M.Y. Visualization: W.Z. Writing – original draft: W.Z. Writing – review & Editing: W.Z., J.W., A.A., N.L.A., D.B., M.Y., D.G. Funding Acquisition: W.Z., A.A., D.G.

Acknowledgement

The research was supported by the Hong Kong Research Grants Council (26304921), Hong Kong Innovation and Technology Fund (ITS/193/20FP), and the Department of Science and Technology of Guangdong Province in China (2019B121205004). J.W. was funded by the UKRI Future Leaders Fellowship Programme (MR/T019867/1) awarded to Dr. Maria Val Martin while at the University of Sheffield. This study contains data supplied by the Natural Environment Research Council. We extend thanks to the British Oceanographic Data Center, Lucy Carpenter, and Monica Hanley for providing isoprene measurements from the cruises AMT22, AMT23, ACCACIA 1, and ACCACIA 2. This work used Monsoon2 (a collaborative High-Performance Computing facility funded by the Met Office and the Natural Environment Research Council) and JASMIN (the UK collaborative data analysis facility).

Supporting Information Available

Section S1: UKESM1 simulations

Section S2: Impact of emission uncertainty on atmospheric composition

Section S3: Uncertainty analysis of marine isoprene emissions

Figure S1 to S21

Table S1 to S5

References

(1) Weber, J.; Archer-Nicholls, S.; Abraham, N. L.; Shin, Y. M.; Griffiths, P.; Grosvenor, D. P.; Scott, C. E.; Archibald, A. T. Chemistry-driven changes strongly influence climate forcing from vegetation emissions. *Nat. Commun.* **2022**, *13*, 7202.

(2) Guenther, A. B.; Jiang, X.; Heald, C. L.; Sakulyanontvittaya, T.; Duhl, T.; Em-

mons, L. K.; Wang, X. The Model of Emissions of Gases and Aerosols from Nature version 2.1 (MEGAN2.1): an extended and updated framework for modeling biogenic emissions. *Geosci. Model Dev.* **2012**, *5*, 1471–1492.

(3) Gaston, C. J.; Riedel, T. P.; Zhang, Z.; Gold, A.; Surratt, J. D.; Thornton, J. A. Reactive Uptake of an Isoprene-Derived Epoxydiol to Submicron Aerosol Particles. *Environ. Sci. Technol.* **2014**, *48*, 11178–11186.

(4) Nguyen, T. B.; Coggon, M. M.; Bates, K. H.; Zhang, X.; Schwantes, R. H.; Schilling, K. A.; Loza, C. L.; Flagan, R. C.; Wennberg, P. O.; Seinfeld, J. H. Organic aerosol formation from the reactive uptake of isoprene epoxydiols (IEPOX) onto non-acidified inorganic seeds. *Atmos. Chem. Phys.* **2014**, *14*, 3497–3510.

(5) Claeys, M.; others Formation of Secondary Organic Aerosols Through Photooxidation of Isoprene. *Science* **2004**, *303*, 1173–1176.

(6) Kroll, J. H.; Seinfeld, J. H. Chemistry of secondary organic aerosol: formation and evolution of low-volatility organics in the atmosphere. *Atmos. Environ.* **2008**, *42*, 3593–3624.

(7) Krechmer, J. E. et al. Formation of Low Volatility Organic Compounds and Secondary Organic Aerosol from Isoprene Hydroxyhydroperoxide Low-NO Oxidation. *Environ. Sci. Technol.* **2015**, *49*, 10330–10339.

(8) Schwantes, R. H.; Charan, S. M.; Bates, K. H.; Huang, Y.; Nguyen, T. B.; Mai, H.; Kong, W.; Flagan, R. C.; Seinfeld, J. H. Low-volatility compounds contribute significantly to isoprene secondary organic aerosol (SOA) under high-NO_x conditions. *Atmos. Chem. Phys.* **2019**, *19*, 7255–7278.

(9) Lamkaddam, H.; Dommen, J.; Ranjithkumar, A.; Gordon, H.; Wehrle, G.; Krechmer, J.; Majluf, F.; Salionov, D.; Schmale, J.; Bjelić, S.; Carslaw, K. S.; El Haddad, I.;

Baltensperger, U. Large contribution to secondary organic aerosol from isoprene cloud chemistry. *Sci. Adv.* **2021**, *7*, eabe2952.

(10) Henze, D. K.; Seinfeld, J. H. Global secondary organic aerosol from isoprene oxidation. *Geophys. Res. Lett.* **2006**, *33*, L09812.

(11) Hoyle, C. R.; Berntsen, T.; Myhre, G.; Isaksen, I. S. A. Secondary organic aerosol in the global aerosol – chemical transport model Oslo CTM2. *Atmos. Chem. Phys.* **2007**, *7*, 5675–5694.

(12) Stadtler, S.; Kühn, T.; Schröder, S.; Taraborrelli, D.; Schultz, M. G.; Kokkola, H. Isoprene-derived secondary organic aerosol in the global aerosol–chemistry–climate model ECHAM6.3.0–HAM2.3–MOZ1.0. *Geosci. Model Dev.* **2018**, *11*, 3235–3260.

(13) Bates, K. H.; Jacob, D. J. A new model mechanism for atmospheric oxidation of isoprene: global effects on oxidants, nitrogen oxides, organic products, and secondary organic aerosol. *Atmos. Chem. Phys.* **2019**, *19*, 9613–9640.

(14) Bonsang, B.; Polle, C.; Lambert, G. Evidence for marine production of isoprene. *Geophys. Res. Lett.* **1992**, *19*, 1129–1132.

(15) Broadgate, W. J.; Liss, P. S.; Penkett, S. A. Seasonal emissions of isoprene and other reactive hydrocarbon gases from the ocean. *Geophys. Res. Lett.* **1997**, *24*, 2675–2678.

(16) Guenther, A.; Karl, T.; Harley, P.; Wiedinmyer, C.; Palmer, P. I.; Geron, C. Estimates of global terrestrial isoprene emissions using MEGAN (Model of Emissions of Gases and Aerosols from Nature). *Atmos. Chem. Phys.* **2006**, *6*, 3181–3210.

(17) Kameyama, S.; Yoshida, S.; Tanimoto, H.; Inomata, S.; Suzuki, K.; Yoshikawa-Inoue, H. High-resolution observations of dissolved isoprene in surface seawater in the Southern Ocean during austral summer 2010–2011. *J. Oceanogr.* **2014**, *70*, 225–239.

(18) Meskhidze, N.; Nenes, A. Phytoplankton and Cloudiness in the Southern Ocean. *Science* **2006**, *314*, 1419–1423.

(19) Hu, Q.; Xie, Z.; Wang, X.; Kang, H.; He, Q.; Zhang, P. Secondary organic aerosols over oceans via oxidation of isoprene and monoterpenes from Arctic to Antarctic. *Sci Rep* **2013**, *3*, 2280.

(20) Hackenberg, S. C. et al. Potential controls of isoprene in the surface ocean: isoprene Controls in the Surface Ocean. *Glob. Biogeochem. Cycle* **2017**, *31*, 644–662.

(21) Booge, D.; Schlundt, C.; Bracher, A.; Endres, S.; Zäncker, B.; Marandino, C. A. Marine isoprene production and consumption in the mixed layer of the surface ocean – a field study over two oceanic regions. *Biogeosciences* **2018**, *15*, 649–667.

(22) Colomb, A.; Yassaa, N.; Williams, J.; Peeken, I.; Lochte, K. Screening volatile organic compounds (VOCs) emissions from five marine phytoplankton species by head space gas chromatography/mass spectrometry (HS-GC/MS). *J. Environ. Monit.* **2008**, *10*, 325.

(23) Exton, D. A.; Suggett, D. J.; McGenity, T. J.; Steinke, M. Chlorophyll-normalized isoprene production in laboratory cultures of marine microalgae and implications for global models. *Limnol. Oceanogr.* **2013**, *58*, 1301–1311.

(24) Shaw, S. L.; Chisholm, S. W.; Prinn, R. G. Isoprene production by Prochlorococcus, a marine cyanobacterium, and other phytoplankton. *Mar. Chem.* **2003**, *80*, 227–245.

(25) Broadgate, W. J.; Malin, G.; Küpper, F. C.; Thompson, A.; Liss, P. Isoprene and other non-methane hydrocarbons from seaweeds: a source of reactive hydrocarbons to the atmosphere. *Mar. Chem.* **2004**, *88*, 61–73.

(26) Meskhidze, N.; Sabolis, A.; Reed, R.; Kamykowski, D. Quantifying environmental

stress-induced emissions of algal isoprene and monoterpenes using laboratory measurements. *Biogeosciences* **2015**, *12*, 637–651.

(27) Simó, R.; Cortés-Greus, P.; Rodríguez-Ros, P.; Masdeu-Navarro, M. Substantial loss of isoprene in the surface ocean due to chemical and biological consumption. *Commun. Earth Environ.* **2022**, *3*, 20.

(28) Novak, G. A.; Bertram, T. H. Reactive VOC Production from Photochemical and Heterogeneous Reactions Occurring at the Air–Ocean Interface. *Accounts Chem. Res.* **2020**, *53*, 1014–1023.

(29) Arnold, S. R.; Spracklen, D. V.; Williams, J.; Yassaa, N.; Sciare, J.; Bonsang, B.; Gros, V.; Peeken, I.; Lewis, A. C.; Alvain, S.; Moulin, C. Evaluation of the global oceanic isoprene source and its impacts on marine organic carbon aerosol. *Atmos. Chem. Phys.* **2009**, *9*, 1253–1262.

(30) Luo, G.; Yu, F. A numerical evaluation of global oceanic emissions of α-pinene and isoprene. *Atmos. Chem. Phys.* **2010**, *10*, 2007–2015.

(31) Palmer, P. I.; Shaw, S. L. Quantifying global marine isoprene fluxes using MODIS chlorophyll observations. *Geophys. Res. Lett.* **2005**, *32*, L09805.

(32) Booge, D.; Marandino, C. A.; Schlundt, C.; Palmer, P. I.; Schlundt, M.; Atlas, E. L.; Bracher, A.; Saltzman, E. S.; Wallace, D. W. R. Can simple models predict large-scale surface ocean isoprene concentrations? *Atmos. Chem. Phys.* **2016**, *16*, 11807–11821.

(33) Conte, L.; Szopa, S.; Aumont, O.; Gros, V.; Bopp, L. Sources and Sinks of Isoprene in the Global Open Ocean: Simulated Patterns and Emissions to the Atmosphere. *J. Geophys. Res.-Oceans* **2020**, *125*, e2019JC015946.

(34) Ciuraru, R.; Fine, L.; Pinxteren, M. V.; D'Anna, B.; Herrmann, H.; George, C. Un-

ravelling New Processes at Interfaces: photochemical Isoprene Production at the Sea Surface. *Environ. Sci. Technol.* **2015**, *49*, 13199–13205.

(35) Brüggemann, M.; Hayeck, N.; George, C. Interfacial photochemistry at the ocean surface is a global source of organic vapors and aerosols. *Nat. Commun.* **2018**, *9*, 2101.

(36) Gantt, B.; Meskhidze, N.; Zhang, Y.; Xu, J. The effect of marine isoprene emissions on secondary organic aerosol and ozone formation in the coastal United States. *Atmos. Environ.* **2010**, *44*, 115–121.

(37) Gantt, B.; Meskhidze, N.; Carlton, A. G. The contribution of marine organics to the air quality of the western United States. *Atmos. Chem. Phys.* **2010**, *10*, 7415–7423.

(38) Zhang, W.; Gu, D. Geostationary satellite reveals increasing marine isoprene emissions in the center of the equatorial Pacific Ocean. *npj Clim. Atmos. Sci.* **2022**, *5*, 83.

(39) Savtchenko, A.; Ouzounov, D.; Ahmad, S.; Acker, J.; Leptoukh, G.; Koziana, J.; Nickless, D. Terra and Aqua MODIS products available from NASA GES DAAC. *Adv. Space Res.* **2004**, *34*, 710–714.

(40) Mulet, S.; Rio, M.-H.; Mignot, A.; Guinehut, S.; Morrow, R. A new estimate of the global 3D geostrophic ocean circulation based on satellite data and in-situ measurements. *Deep Sea Res. Part II Top. Stud. Oceanogr.* **2012**, *77-80*, 70–81.

(41) Guinehut, S.; Dhomps, A.-L.; Larnicol, G.; Le Traon, P.-Y. High resolution 3-D temperature and salinity fields derived from in situ and satellite observations. *Ocean Sci.* **2012**, *8*, 845–857.

(42) Hersbach, H. et al. The ERA5 global reanalysis. *Q. J. R. Meteorol. Soc.* **2020**, *146*, 1999–2049.

(43) Correa-Ramirez, M.; Morales, C.; Letelier, R.; Anabalón, V.; Hormazabal, S. Improving the Remote Sensing Retrieval of Phytoplankton Functional Types (PFT) Using Em-

pirical Orthogonal Functions: A Case Study in a Coastal Upwelling Region. *Remote Sens.* **2018**, *10*, 498.

(44) Moore, R. M.; Wang, L. The influence of iron fertilization on the fluxes of methyl halides and isoprene from ocean to atmosphere in the SERIES experiment. *Deep Sea Res. Part II Top. Stud. Oceanogr.* **2006**, *53*, 2398–2409.

(45) Gantt, B.; Meskhidze, N.; Kamykowski, D. A new physically-based quantification of marine isoprene and primary organic aerosol emissions. *Atmos. Chem. Phys.* **2009**, *9*, 4915–4927.

(46) Wanninkhof, R. Relationship between wind speed and gas exchange over the ocean revisited: gas exchange and wind speed over the ocean. *Limnol. Oceanogr. Meth.* **2014**, *12*, 351–362.

(47) Rodríguez-Ros, P.; Galí, M.; Cortés, P.; Robinson, C. M.; Antoine, D.; Wohl, C.; Yang, M.; Simó, R. Remote Sensing Retrieval of Isoprene Concentrations in the Southern Ocean. *Geophys. Res. Lett.* **2020**, *47*, e2020GL087888.

(48) Brüggemann, M.; Hayeck, N.; Bonnineau, C.; Pesce, S.; Alpert, P. A.; Perrier, S.; Zuth, C.; Hoffmann, T.; Chen, J.; George, C. Interfacial photochemistry of biogenic surfactants: a major source of abiotic volatile organic compounds. *Faraday Discuss.* **2017**, *200*, 59–74.

(49) Escobedo, J. F.; Gomes, E. N.; Oliveira, A. P.; Soares, J. Ratios of UV, PAR and NIR components to global solar radiation measured at Botucatu site in Brazil. *Renew. Energy* **2011**, *36*, 169–178.

(50) Ciuraru, R.; Fine, L.; van Pinxteren, M.; D'Anna, B.; Herrmann, H.; George, C. Photosensitized production of functionalized and unsaturated organic compounds at the air-sea interface. *Sci Rep* **2015**, *5*, 12741.

(51) Wurl, O.; Wurl, E.; Miller, L.; Johnson, K.; Vagle, S. Formation and global distribution of sea-surface microlayers. *Biogeosciences* **2011**, *8*, 121–135.

(52) McGillis, W. R.; Edson, J. B.; Zappa, C. J.; Ware, J. D.; McKenna, S. P.; Terray, E. A.; Hare, J. E.; Fairall, C. W.; Drennan, W.; Donelan, M.; DeGrandpre, M. D.; Wanninkhof, R.; Feely, R. A. Air-sea CO_2 exchange in the equatorial Pacific. *J. Geophys. Res.: Oceans* **2004**, *109*, 2003JC002256.

(53) Sabbaghzadeh, B.; Upstill-Goddard, R. C.; Beale, R.; Pereira, R.; Nightingale, P. D. The Atlantic Ocean surface microlayer from 50°N to 50°S is ubiquitously enriched in surfactants at wind speeds up to 13 m s^{-1}. *Geophys. Res. Lett.* **2017**, *44*, 2852–2858.

(54) Weber, J.; Archer-Nicholls, S.; Abraham, N. L.; Shin, Y. M.; Bannan, T. J.; Percival, C. J.; Bacak, A.; Artaxo, P.; Jenkin, M.; Khan, M. A. H.; Shallcross, D. E.; Schwantes, R. H.; Williams, J.; Archibald, A. T. Improvements to the representation of BVOC chemistry–climate interactions in UKCA (v11.5) with the CRI-Strat 2 mechanism: incorporation and evaluation. *Geosci. Model Dev.* **2021**, *14*, 5239–5268.

(55) Jenkin, M.; Khan, M.; Shallcross, D.; Bergström, R.; Simpson, D.; Murphy, K.; Rickard, A. The CRI v2.2 reduced degradation scheme for isoprene. *Atmos. Environ.* **2019**, *212*, 172–182.

(56) Mann, G. W.; Carslaw, K. S.; Spracklen, D. V.; Ridley, D. A.; Manktelow, P. T.; Chipperfield, M. P.; Pickering, S. J.; Johnson, C. E. Description and evaluation of GLOMAP-mode: a modal global aerosol microphysics model for the UKCA composition-climate model. *Geosci. Model Dev.* **2010**, *3*, 519–551.

(57) Mulcahy, J. P. et al. Description and evaluation of aerosol in UKESM1 and HadGEM3-GC3.1 CMIP6 historical simulations. *Geosci. Model Dev.* **2020**, *13*, 6383–6423.

(58) Archibald, A. T. et al. Description and evaluation of the UKCA strato-

sphere–troposphere chemistry scheme (StratTrop vn 1.0) implemented in UKESM1. *Geosci. Model Dev.* **2020**, *13*, 1223–1266.

(59) Telford, P. J.; Braesicke, P.; Morgenstern, O.; Pyle, J. A. Technical Note: Description and assessment of a nudged version of the new dynamics Unified Model. *Atmos. Chem. Phys.* **2008**, *8*, 1701–1712.

(60) Dee, D. P. et al. The ERA-Interim reanalysis: configuration and performance of the data assimilation system. *Q. J. R. Meteorol. Soc.* **2011**, *137*, 553–597.

(61) Mulcahy, J. P. et al. UKESM1.1: development and evaluation of an updated configuration of the UK Earth System Model. *Geosci. Model Dev.* **2023**, *16*, 1569–1600.

(62) Archibald, A. T. et al. Tropospheric Ozone Assessment Report. *Elementa-Sci. Anthrop.* **2020**, *8*, 034.

(63) Pacifico, F.; Harrison, S.; Jones, C.; Sitch, S. Isoprene emissions and climate. *Atmos. Environ.* **2009**, *43*, 6121–6135.

(64) Kenagy, H. S.; Heald, C. L.; Tahsini, N.; Goss, M. B.; Kroll, J. H. Can we achieve atmospheric chemical environments in the laboratory? An integrated model-measurement approach to chamber SOA studies. *Sci. Adv.* **2024**, *10*, eado1482.

(65) Shrivastava, M. et al. Recent advances in understanding secondary organic aerosol: implications for global climate forcing. *Rev. Geophys.* **2017**, *55*, 509–559.

(66) Bardakov, R.; Thornton, J. A.; Riipinen, I.; Krejci, R.; Ekman, A. M. L. Transport and chemistry of isoprene and its oxidation products in deep convective clouds. *Tellus Ser. B-Chem. Phys. Meteorol.* **2021**, *73*, 1979856.

(67) Wolf, M. J. et al. A biogenic secondary organic aerosol source of cirrus ice nucleating particles. *Nat. Commun.* **2020**, *11*, 4834.

(68) Shen, J. et al. New particle formation from isoprene under upper-tropospheric conditions. *Nature* **2024**, *636*, 115–123.

(69) Curtius, J. et al. Isoprene nitrates drive new particle formation in Amazon's upper troposphere. *Nature* **2024**, *636*, 124–130.

(70) King, A. C. F.; Thomas, E. R.; Pedro, J. B.; Markle, B.; Potocki, M.; Jackson, S. L.; Wolff, E.; Kalberer, M. Organic Compounds in a Sub-Antarctic Ice Core: A Potential Suite of Sea Ice Markers. *Geophys. Res. Lett.* **2019**, *46*, 9930–9939.

(71) Thornhill, G. et al. Climate-driven chemistry and aerosol feedbacks in CMIP6 Earth system models. *Atmos. Chem. Phys.* **2021**, *21*, 1105–1126.

TOC Graphic

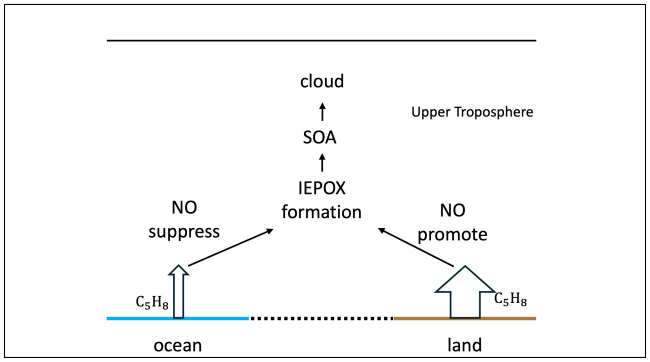
cloud
Upper Troposphere
SOA
IEPOX
formation
NO
suppress
NO
promote
C_5H_8
C_5H_8
ocean
land